

## SUPERHYDROPHOBIC SURFACES FOR DRAG REDUCTION

ALESSANDRO BOTTARO (\*)

Nota presentata dal m.e. Alfio Quarteroni  
(Adunanza del 27 novembre 2014)

SUNTO. – Le proprietà dei materiali superidrofobici sono esaminate alla luce del loro possibile uso per la riduzione di attrito in applicazioni navali. La superidrofobicità può essere raggiunta strutturando un materiale di bassa energia superficiale in modo da minimizzare le interazioni solido-liquido. L'aspetto cruciale che deve essere considerato è quello del mantenimento di uno strato di gas inframezzato tra la parete (caratterizzata da asperità superficiali) e il liquido, attraverso l'uso di una micro- e nano-strutturazione della superficie solida, di modo che il liquido possa *scorrere* sulla parete con conseguente riduzione dell'attrito. Il comportamento del liquido è quantificato da una *lunghezza di scorrimento* il cui valore, secondo recenti risultati sperimentali, può raggiungere anche i 400  $\mu\text{m}$ . Per il fenomeno della transizione verso la turbolenza si mostra che le superfici superidrofobiche sono efficaci (cioè ritardano la destabilizzazione di onde viaggianti nel canale) unicamente per condotti dalle dimensioni caratteristiche di pochi millimetri. La situazione è diversa se il moto fluido ha già raggiunto uno stato turbolento, e una riduzione molto significativa della resistenza può essere ottenuta anche in configurazioni macroscopiche. Ciò accade in quanto la scala di lunghezza caratteristica dello strato limite è ora lo spessore del sottostrato viscoso, che può essere di taglia paragonabile alla lunghezza di scorrimento, così che interazioni positive possono emergere. Infine, alcune procedure di produzione di superfici superidrofobiche vengono esaminate, alla luce della possibilità di applicare tali rivestimenti innovativi sulla chiglia di imbarcazioni.

\*\*\*

ABSTRACT. – Properties of superhydrophobic materials are examined in light of their possible use for drag reduction in naval applications. To achieve superhydrophobicity

---

(\*) DICCA, Scuola Politecnica, Università di Genova, Via Montallegro 1, 16145 Genova, Italy.  
E-mail: [alessandro.bottaro@unige.it](mailto:alessandro.bottaro@unige.it)

a low-surface-energy material must be structured so as to minimize the liquid-solid interactions. The crucial aspect is that of maintaining a layer of gas in between the (rough) wall and the liquid, and this can be achieved by hierarchical micro- and nano-structuring of the solid surface, to ensure a sufficiently large *apparent* slip of the fluid at the wall, thus reducing skin friction. The behavior of the liquid is quantified by a *slip length*; recent results have shown that this length can be as large as  $400\ \mu\text{m}$ . As far as transition to turbulence is concerned, we show that superhydrophobic surfaces are effective (*i.e.* they delay the onset of travelling instability waves) only in channels with characteristic dimensions of a few millimeters. Conversely, when the fluid flow has already attained a turbulent state, the gain in term of drag reduction can be very significant also in macroscopic configurations. This occurs because the relevant length scale of the boundary layer is now the thickness of the viscous sub-layer, which can be of magnitude comparable to the slip length, so that an effective coupling emerges. Finally, some procedures to produce superhydrophobic surfaces are examined, in light of the possible application of such innovative coatings on the hull of ships.

## 1. INTRODUCTION

Biological surfaces are never smooth but covered with hair, filaments, scales, feathers, leaves, needles, cilia, etc., which perform a variety of functions. Such *appendages* often have only local interactions with the fluid flowing over or around them, so that the effect produced is circumscribed over distances which can be rather small. In other instances, surface irregularities (say, an array of short filaments) can produce an effect of much larger scale, because of their collective behavior. The example that comes to mind immediately is that of flexible plant canopies, with the wind above the canopy forming eddies which drive *honami* waves.<sup>1,2</sup> The plant bending stiffness plays a role in the frequency and wavelength selection of the coherent motion of the canopy. This leads us to a second point: biological surfaces are rarely infinitely rigid, most often they display a visible degree of elasticity, reacting to the stress exerted upon them by the flowing medium. A showcase of the coupled effect of small-scale surface roughness and long-scale compliant behavior is the shark. The shark skin is covered with scales, called denticles, of characteristic length equal to  $100\ \mu\text{m}$ . By mechanically flapping sheets of actual shark skin in a hydrodynamic channel, Oeffner & Lauder<sup>3</sup> have shown that the flow resistance actually increases in the presence of denticles, compared to the case in which denticles are sanded off, when the sheets are maintained rigid. Conversely, a significant drag reduction is achieved for flexible sheets which mimic typical shark undulations. Very recently, the same conclusions have been reached by

the use of artificial denticles made by a 3D printer and embedded in a flexible substrate.<sup>4</sup>

Despite these biomimetic pointers, man insists on conceiving devices and machines which are often as rigid and smooth as possible. An example is constituted by the hull of marine vessels, which undergoes lengthy milling and sanding operations in naval workshops, before painting. Can these operations be carried out so as to prepare the surface “optimally” for the successive coating work? Can the paint itself possess properties able to yield positive hydrodynamic effects (*i.e.* drag reduction)? If such a paint were also capable of reducing or eliminating fouling caused by organisms such as oysters, barnacles, mussels or algae which attach to the hull while the boat is at dock, the advantage would be double, since fouling organisms not only damage the hull, but also cause additional drag and alter the vessel’s maneuverability.

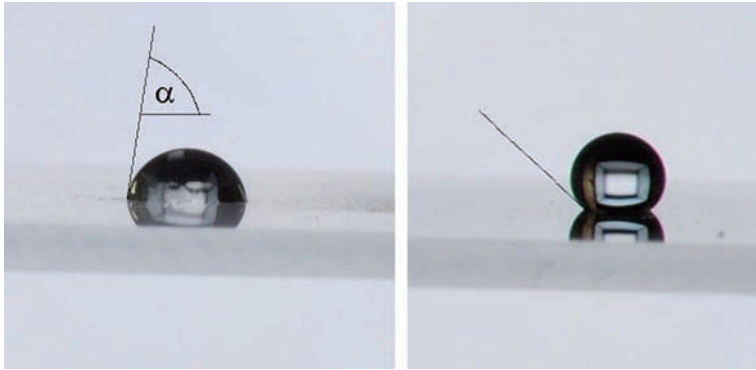
Superhydrophobic (SH in the following) materials have received tremendous attention in recent years for the large variety of applications in which they could be put to profitable use, ranging from anti-wetting to anti-icing, from self-cleaning to anti-corrosion. Examples range from the protection of electrical equipment and the prevention of shortages, to the protection from damage and corrosion of metal, wood or fabrics, the buildup of ice on airplane wings or transmission lines, the cleaning of cars’ windshields or shower doors, etc. The potential application of SH coatings to marine vessels for drag reduction and antifouling is presently acquiring momentum.

### 1.1 Some definitions

A SH surface is initially defined on the basis of static conditions; *Fig. 1* shows two water drops which have been gently deposited onto two identical glass surfaces, the second of which has been treated with a SH coating. The difference is striking, including the fact that the glass in the second case is not perfectly smooth any more.

The *apparent*,<sup>5</sup> static contact angle  $\alpha$  exhibited at a stationary contact line depends *uniquely* on the characteristics of the three materials involved, *i.e.* the gas, the liquid and the solid, reflecting the nature of the interactions at the different surfaces which intersect at the contact line. It is useful to introduce a quantity,  $\gamma_{AB}$ , called interfacial or surface energy, which represents the work per unit area required to increase the surface area of substance *A* in contact with substance *B*. The interfacial

energy of a condensed material derives from the unsatisfied bonding potential of the molecules at its surface: the higher the surface energy of a solid, the higher its ability to bond with other materials. The degree of wetting (*viz.* the wettability) of a solid by water arises from a balance between adhesive forces (*i.e.* solid-liquid interactions) and cohesive forces within the liquid. Water has a *strong attraction* for itself (strong cohesive forces) and wettability is thus determined by the interfacial energy of the solid. Molecules of materials such as fluoropolymers are held together by weak forces; such materials have low surface energy and low wettability. Conversely, metals, glass and ceramic materials have high surface energy, because of strong chemical bonds, and thus high wettability.



*Fig. 1 – A small drop of water deposited onto clean glass (left) displays an apparent contact angle  $\alpha$  smaller than  $90^\circ$ , whereas a drop deposited onto the same glass sprayed with carbon nanotubes shows a much larger contact angle.  
Pictures courtesy of Nicolas Mazellier.*

With reference to *Fig. 2*, a static force balance at the solid-liquid-gas contact line in the plane of the solid boundary, first proposed by Young<sup>6</sup> for a perfectly smooth, planar and chemically homogeneous solid surface, yields

$$A = \gamma_{SG} - \gamma_{LS} = \gamma_{GL} \cos \alpha, \quad (1)$$

with  $A$  the adhesion tension, and subscripts  $L$ ,  $G$  and  $S$  denoting, respectively, the liquid, gas and solid phase. A value of  $\alpha$  between  $0^\circ$  and  $90^\circ$  (high wettability) means that the liquid is strongly attracted to the solid,

which is thus called hydrophilic; when  $\alpha$  exceeds  $90^\circ$  (low wettability) the surface is said to be hydrophobic.<sup>7</sup> When the apparent contact angle exceeds  $150^\circ$  the surface is called superhydrophobic, provided the contact angle hysteresis  $\Delta\alpha$  (see later for definition) does not exceed  $5^\circ$ . The simple equation (1) above is, however, of little practical use since it is very difficult to measure directly either  $\gamma_{LS}$  or  $\gamma_{SG}$ ; conversely,  $\gamma_{GL}$  is easily measurable and is denoted simply by  $\gamma$ ; its value, the so-called *surface tension*, equals  $0.073 \text{ N m}^{-1}$  for the case of an air-water interface at  $20^\circ\text{C}$ . A further limitation of Young's equation lies in the fact that, when the drop is micro or nanometric,  $\alpha$  depends on the drop size.<sup>8</sup>

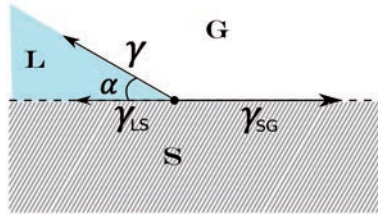


Fig. 2 – Static force balance at a triple line.

A low-surface-energy material is the first condition for superhydrophobicity. The second condition rests on the roughness or surface topography produced by fabrication and coating processes.

Wenzel<sup>9</sup> was the first to study the wetting characteristics of rough materials, with a focus on woven or knitted fabrics to be made waterproof. He argued that, for the case of a real (*viz.* rough) solid,  $A$  in equation (1) must be replaced by an *effective adhesion tension* given by the product of  $A$  with a roughness factor,  $r$ , which expresses the ratio of the actual surface of the interface to its planar projection, *i.e.*

$$rA = \gamma \cos \alpha_w, \quad (2)$$

with  $r \geq 1$ . Whereas  $A$  depends solely on the chemical composition of the three contiguous phases, the effective adhesion tension  $rA$  varies widely with the microscopic morphology of the solid;  $rA$  is the value typically measured experimentally. According to this simplified model, the equilibrium contact angle in the Wenzel state,  $\alpha_w$ , is given by

$$\cos \alpha_w = r \cos \alpha; \quad (3)$$

the presence of the parameter  $r$  indicates that roughness reinforces hydrophobicity (as well as hydrophilicity) with respect to a smooth surface. Discussions on the applicability and limitations of the Wenzel model are provided by Wolansky & Marmur<sup>10</sup> and Gao & McCarthy,<sup>11</sup> with particular reference to the possible pinning of the contact line along defects on the surface and the effect of chemical and geometrical properties of the interfacial area contained within the contact perimeter. Despite criticisms, Wenzel's averaged view represents a useful scheme for uniformly rough surfaces and for drops much larger than the length scale of surface heterogeneities.

One aspect which complicates the understanding of wetting phenomena is the so-called contact angle hysteresis, which manifests itself, for example, when droplets on an incline remain at rest, with the front and rear contact angles exhibiting different values. The asymmetry in contact angles creates a Laplace pressure difference between the front of the drop (high curvature and high pressure) and the rear (small curvature and small pressure) so that the weight of the drop might be balanced. Even in this case chemical heterogeneities and roughness can act as pinning sites, so that the hysteresis  $\Delta\alpha = \alpha_a - \alpha_r$  depends strongly on surface properties ( $\alpha_a$  and  $\alpha_r$  denote, respectively, the advancing and receding contact angles). Eventually, should the angle of the incline exceed a certain threshold value, the drop slides down, maintaining a front-rear asymmetry.

If air is trapped within asperities, so that the solid-liquid contact area is decreased, ultra- or super-hydrophobicity can be attained, with the drop partially *sitting* on air (this is known as the Cassie-Baxter<sup>12</sup> or fakir<sup>13,14</sup> state). Capturing and maintaining a connected gas layer (or disconnected gas bubbles) between the solid and the liquid depends crucially on the way the solid surface is structured. Cassie & Baxter<sup>12</sup> have proposed the following equation to describe the contact angle  $\alpha_F$  in the fakir state:

$$\cos \alpha_F = f_1 \cos \alpha - f_2, \quad (4)$$

with  $f_1$  the total area of solid per unit projected area under the liquid and  $f_2$  defined in an analogous way for the air-liquid interface. The two-dimensional schematic in *Fig. 3* clarifies the definition of  $f_1$  and  $f_2$  for coplanar interfaces (left image) and for the case in which water partially fills the cavities. The Cassie-Baxter equation captures the Wenzel equation (2) when the air layer disappears, *i.e.* when  $f_1 \rightarrow r$  and  $f_2 \rightarrow 0$ , so that  $\cos \alpha_F = \cos \alpha_W = r \cos \alpha$ . When the solid surface is homogeneous

and smooth ( $r \rightarrow 1$ ) it is correctly recovered that  $\alpha_F = \alpha_W = \alpha$ .

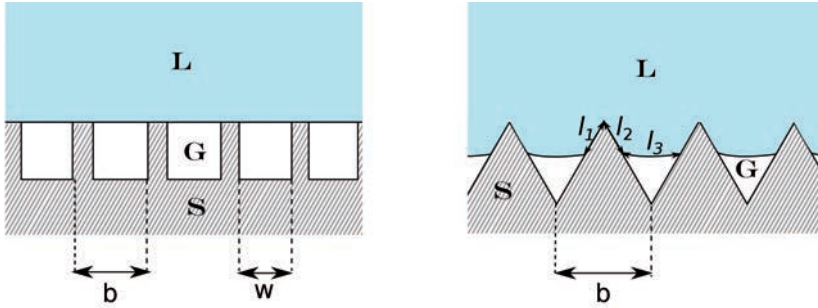


Fig. 3 – Close up of two (periodic) rough surfaces, taken to be homogeneous in the third direction. In the left frame, with reference to equation (4) it is  $f_1 = 1 - w/b$  and  $f_2 = w/b$ , whereas in the right frame  $f_1 = (l_1 + l_2)/b$  and  $f_2 = l_1/b$ .

Sketches of a liquid interacting with a solid in Wenzel and Cassie-Baxter modes are shown in Fig. 4, together with a qualitative sketch of the situation which might take place when the solid surface is both micro- and nano-structured. For simply micro-structured surfaces, the Cassie-Baxter state (left image) can undergo a *wetting transition* with a rapid depletion of the gas layer (or of the gas bubbles), so that the Wenzel mode ensues (center image). In static conditions, this occurs above a critical pressure difference between the liquid and the gas, function of the roughness scale, of surface tension  $\gamma$ , and of the contact angle  $\alpha$ . Furthermore, even for a liquid pressure below critical, the transition to the Wenzel state can still take place, over longer time scales, because of the solubility of gases in water, chemical reactions or Marangoni effects.

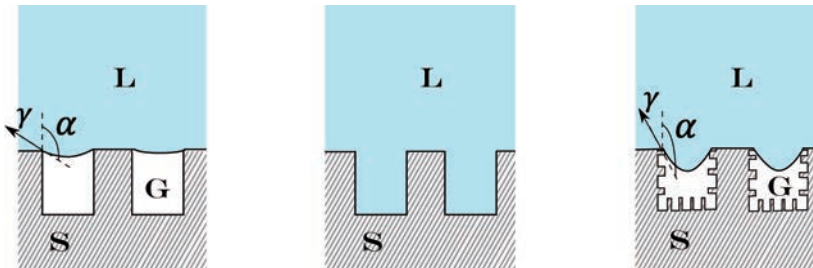


Fig. 4 – From left to right: Cassie-Baxter state with microstructured roughness; Wenzel state; Cassie-Baxter state with micro- and nano-structured roughness. In the latter case, the contact angle  $\alpha$  approaches  $180^\circ$ , so that surface tension  $\gamma$  can more easily balance the pressure difference ( $P_L - P_G$ ).



Hierarchically nanostructured sidewalls yield larger contact angles<sup>15,16</sup> and render the unwetted state more energetically stable<sup>17,18</sup> so that the transition to the Wenzel state is avoided, or at least postponed to larger values of the water pressure (*Fig. 4*, right). By careful design of the micro- and nano-textures, Lee & Kim<sup>16</sup> have been able to achieve a *slip length* (defined later in Section II) of up to 400  $\mu\text{m}$ , rendering feasible the use of SH coatings in macroscale applications.

The key issue which emerges when attempting to design effective SH materials for specific applications is thus the following: how to best structure the surface in order to achieve large slip lengths while avoiding the wetting transition? Unfortunately, requirements on the slip length (and thus on the characteristic length scale  $b$  of the micro-roughness) and on the wetting transition are conflicting, since the collapse pressure  $\Delta P$  at which transition occurs scales like  $\gamma/b$ . It is at this point convenient to turn to Nature.

## 1.2. Biomimicry

*Biomimetics or biomimicry is the imitation of the models, systems, and elements of nature for the purpose of solving complex human problems.*

Wikipedia

The most complete open-source database of biological literature, organized by design and engineering function, is probably the website <http://www.asknature.org/>, initiated in 2008 by Dr. Janine Benyus, founder of the Biomimicry Institute (<http://biomimicry.net/about/biomimicry38/institute/>). When searching for inventive and original solutions to a technical problem, this is the number one stop.

A natural example of water-repellence, known for a long time, is constituted by birds' feathers. In 1944, Cassie & Baxter<sup>12</sup> state that

*it is usually taken for granted that the duck uses an oil or similar coating with larger contact angles than any known to man. In actual fact, the duck obtains its water-repellency from the structure of its feathers.*

After describing how feathers are made, each with a keratin rachis, barbs and tiny barbules, the latter hooked to one another to form a network of fibers (*cf. Fig. 5*, left), Cassie & Baxter conclude that



man's attempts to make clothing with the water-repellency of a duck should be directed to perfecting an appropriate cloth structure rather than as at present, to searching for an improved water-repellent agent.

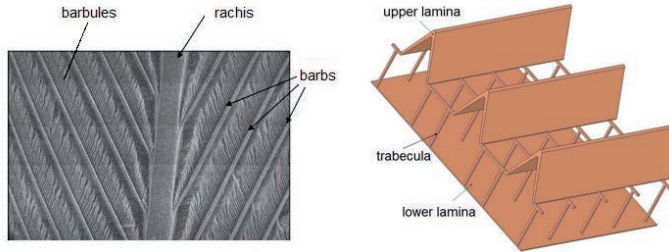


Fig. 5 – Left: scanning electron micrograph (SEM) image of the central part of a feather. The distance between consecutive barbs is of the order of  $200\ \mu\text{m}$ , whereas the spacing between adjacent barbules is of the order of  $10\ \mu\text{m}$ . Figure from Bormasbenko et al.<sup>19</sup> Right: sketch of the structure of a scale of a butterfly wing. Air can flow through the porous interface from the upper lamina to the inner, impermeable region (lower lamina). The upper lamina consists of ridges, of periodicity close to  $2\ \mu\text{m}$ , and grooves with discrete openings, which allow air to flow through. The two laminae are maintained separated by post-like structures, called trabeculae.

Today it is believed that it is the two-scale structure of the feather vane which renders it exceptionally waterproof, with air trapped underneath the network of barbs and barbules.<sup>19</sup>

Man's fascination with superhydrophobicity started probably in 1997 with the work by Barthlott & Neinhuis<sup>20</sup> on the lotus (*Nelumbo nucifera*) leaf. Since then, the number of scientific articles on the *lotus effect* has grown exponentially, and there is still no sign of an approaching saturation. As shown in Fig. 6 (left image) the surface of the lotus leaf has a two-scale structure: the papillose epidermal cells have characteristic dimensions close to  $10\ \mu\text{m}$ , and hairlike epicuticular wax crystalloids sitting on top of the epidermal cells are about  $100\ \text{nm}$  long. The two-level hierarchical surface structure is responsible for the remarkable stability of the Cassie-Baxter state for the lotus leaf even under harsh environmental conditions.<sup>15,17,21</sup>

Another plant which has received recent attention is the water fern *Salvinia molesta*.<sup>22</sup> The surface of the leaf of this plant has a dense coating of elastic hairs shaped as egg-beaters and coated with nanoscopic wax crystals (cf. Fig. 6, right). The terminal cells of each hair lack the crystals, rendering the surface locally hydrophilic (over a por-

tion of approximately 2% of the whole leaf surface). These evenly distributed hydrophilic patches are capable to pin and stabilize the air-water interface, preventing the loss of air for a few weeks even in turbulent flow conditions.

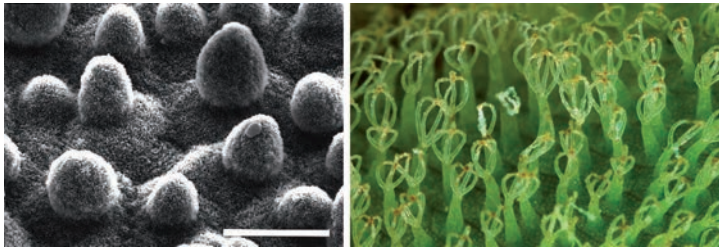


Fig. 6 – Left: SEM image of the lotus leaf. The white bar is 20  $\mu\text{m}$  long. Image from Barthlott and Neinhuis.<sup>20</sup> Right: surface of the leaf of the *Salvinia molesta*. The terminal structure of each egg-beater is half a millimeter wide. Image: [www.invasive.org](http://www.invasive.org).

Interesting SH abilities have been found also among insects. The surface of the legs of the water strider *Gerris remigis*<sup>23,24</sup> displays a hierarchical micro- and nano-structure, with needle-shaped setae oriented longitudinally, of length around 100  $\mu\text{m}$  and diameter ranging from several hundred nanometers to 3  $\mu\text{m}$ ; each seta has elaborate nanoscale grooves. The action of the setae is that of allowing the insect to stand effortlessly and maneuver quickly on water.

Another insect which has shown remarkable properties is the *Natonecta glauca*. Ditsche-Kuru *et al.*<sup>25</sup> have analyzed different body parts of this hairy water bug, to infer that the hierarchical structure formed by setae (of length around 90  $\mu\text{m}$ ) and dense tiny microtrichia (of length close to 2  $\mu\text{m}$ ) on the upper side of the elytra confers tremendous advantages in terms of long term air film persistence (after 130 days under water the air film was marginally altered), for both hydrostatic and hydrodynamic conditions.

A two-scale hierarchical structure appears also on the wings of butterflies and moths. They have wings covered with millions of tiny scales (similar to partially overlapping tiles on a roof) of characteristic dimensions around 100  $\mu\text{m}$ . Scales are made of chitin, a hydrophobic material with contact angle  $\alpha$  close to 100°. Each scale is composed by a riblet-like air-permeable surface, as sketched in Fig. 5 (right frame). By analyzing several species of common butterflies via scanning elec-

tron microscopy and a video optical contact angle measuring system, Fang *et al.*<sup>26</sup> have demonstrated that superhydrophobicity is attained (apparent contact angles increase by up to 40% compared to the base value of chitin) because of the hierarchical nature of the wing structure.

The surface structure of butterfly scales shown in *Fig. 5* (right) resembles that of riblets.<sup>27-29</sup> However, both the function and the mechanism by which riblets operate are different: riblets are completely wetted by the fluid and are used to reduce turbulent friction drag by disrupting the lateral motion of the fluid at the surface, thereby moving turbulent near-wall structures farther from the wall. Furthermore, riblets perform well only in a narrow range of Reynolds numbers, with negative effects outside of their designed range. In particular, they are effective when their spanwise periodicity  $b$  is around 20 viscous wall units (*i.e.* four times the thickness of the turbulent viscous sublayer); in physical units, for the turbulent flow of water in a channel of thickness  $2H = 4 \text{ cm}$  at a bulk velocity of  $0.15 \text{ m s}^{-1}$  (the Reynolds number based on half-channel height is 3000, and the friction velocity  $u_\tau$  is about  $10 \text{ mm s}^{-1}$ ), this translates into a length of the order of  $2 \text{ mm}$ , which is much larger than typical superhydrophobic microfeatures. With the increase of the fluid velocity the thickness of the viscous sublayer decreases, approaching the surface roughness length scale.

### 1.3 Man-made SH surfaces

A large variety of methods have been developed to fabricate non-wettable surfaces, all based on combining a low-surface-energy material with a rough surface morphology; recent reviews are due to Ma & Hill,<sup>30</sup> Zhang *et al.*,<sup>31</sup> and Shirtcliffe, McHale & Newton.<sup>32</sup> Materials of choice for designing, developing and producing superhydrophobic surfaces are polymers; they are versatile, have excellent surface properties and can be easily formed. The softness of polymers, which renders them vulnerable to damage and wear, can be compensated by combining them with inorganic fillers.

In the context of laboratory experiments, SH surfaces are often realized using microfabrication processes developed for the electronic industry, leading to regular arrays of microposts or microridges (*cf. Fig. 7*). For example, photolithographic processes were employed by Daniello,<sup>33</sup> Lee & Kim<sup>34</sup> and Park, Sun & Kim.<sup>35</sup> Large-scale manufacturing of microfabricated SH surfaces is, however, prohibitively expensive. Likewise,

the cost and the complexity of electrospinning techniques,<sup>36,37</sup> together with the need of a high voltage source and the slow rate of fiber production, limit the appeal of electrospun fibers.

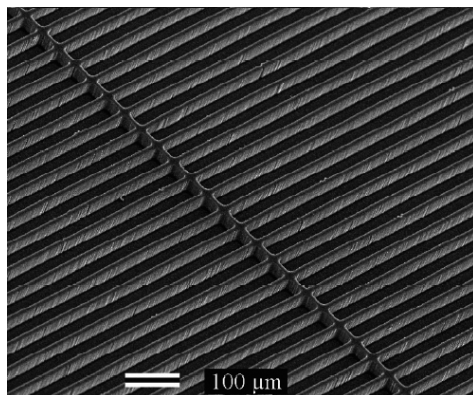


Fig. 7 – Scanning electron micrograph of microridges. The flow runs along the microridges, from bottom left to top right. The single transverse ridge in the image is meant to trap the air layer and ensure its longevity. Figure from Daniello.<sup>33</sup>

A low cost alternative is the one-step casting technique described by Buatier de Mongeot *et al.*<sup>38</sup> and Hsu & Sigmund,<sup>39</sup> with a membrane filter as the mold. In the former study, a disordered array of poly(dimethyl)siloxane micro-pillars hinged on a substrate of the same material was achieved. In the latter, polycarbonate hairs were cast on a polypropylene substrate. In both cases excellent hydrophobic properties were achieved, related to the mechanical response (deflection) of the pillars to the fluid interface. The limitation of this casting approach lies at present in the little resistance of the fibrous structures to abrasion, and the difficulty of producing large scale samples, for example for naval applications.

Another alternative is constituted by spray deposition, which allows to rapidly and conformally coat large areas on a variety of substrates; Srinivasan *et al.*<sup>40</sup> describe a simple spraying technique of poly(methyl methacrylate) blends to fabricate microtextured, superoleophobic surfaces with re-entrant topographic features, capable to enhance the stability of the Cassie-Baxter state. When using this spray-coating technique onto various woven wire meshes (an example of which is shown in Fig. 8) a dual texture is achieved which, in laminar flow conditions, allows to significantly increase the apparent slip of the

fluid at the wall.<sup>41</sup> It appears interesting also the possibility to incorporate aerogel particles into polymer mixtures to be directly painted or sprayed onto the solid surface.<sup>42</sup>

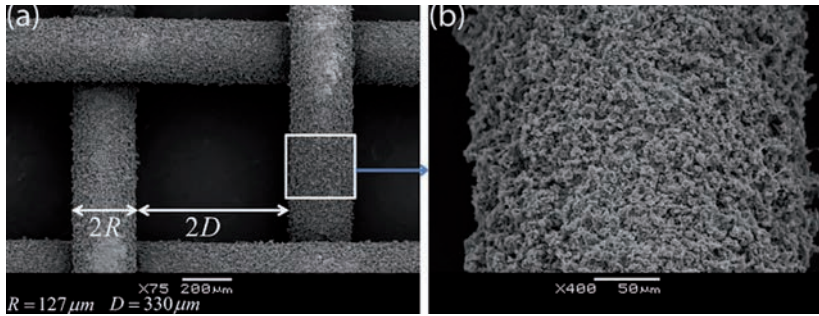


Fig. 8 – SEM image at two magnifications of a dual-textured spray-coated SH mesh surface. Figure from Srinivasan et al.<sup>40</sup>

Probably the simplest technique consists in the direct mechanical abrasion of the surface of a low-surface-energy material, as proposed by Nilsson, Daniello & Rothstein;<sup>43</sup> they have used various grits of sandpaper to treat smooth surfaces made of polytetrafluoroethylene (commercially known as Teflon), measuring contact angles and contact angle hystereses to catalogue the surfaces obtained. Experiments in a microchannel under laminar flow conditions, carried out very recently by Song, Daniello & Rothstein,<sup>44</sup> have employed a variety of such surfaces to infer a correlation between the surface with lower hysteresis (produced by sandpaper with gritsize denominated 240-grit) and the largest pressure drop reduction in the channel (up to 27%, when the sanding is done in the direction of the flow). These results are very promising in view of potential applications because of the large surface areas which can be treated easily and cheaply.

## 2. TO SLIP OR NON TO SLIP?

One of the crucial *assumptions*, based mostly on empirical evidence, made in fluid dynamics is that the molecules composing the liquid adhere to the impermeable wall about which the fluid moves. If  $\Gamma$  is the solid surface of unit normal vector  $\mathbf{n}$ , directed into the fluid, in the frame of reference fixed with the wall we are accustomed to writing:

$$\mathbf{u} \cdot \mathbf{n} = 0, \quad \mathbf{u}_{\parallel} = \mathbf{u} - (\mathbf{u} \cdot \mathbf{n})\mathbf{n} = 0, \quad \text{both valid at } \Gamma,$$

with  $\mathbf{u}$  the fluid velocity and  $\mathbf{u}_{\parallel}$  the vector of velocity components tangent to the surface. The no-slip condition has been questioned for a long time, and has become a tenet in fluid mechanics only after 1923, following G.I. Taylor<sup>45</sup> use of it, and success in relating theory and experiments in the analysis of the stability of Taylor-Couette flow. One hundred years earlier, Navier<sup>46</sup> had proposed another condition for the tangential velocity (with no more theoretical foundation than the no-slip condition, only more general), *i.e.*

$$\mathbf{u}_{\parallel} = 2\lambda\{\mathbf{E} \cdot \mathbf{n} - [(\mathbf{E} \cdot \mathbf{n}) \cdot \mathbf{n}] \mathbf{n}\}, \quad \text{at } \Gamma, \quad (5)$$

with  $\mathbf{E} \equiv \frac{1}{2}(\nabla\mathbf{u} + \nabla\mathbf{u})$  the rate of strain tensor. The parameter  $\lambda$  is known as the *slip length*, the fictitious distance below the reference surface where the velocity of a flowing liquid vanishes (*cf.* Fig. 9); the classical no-slip condition is recovered for  $\lambda = 0$  and perfect slip is found for  $\lambda \rightarrow \infty$ . In equation (5) a unique slip length is employed for the two wall-tangent velocity components; for the case of anisotropic SH surfaces (for example, when the wall has microridges aligned with the main flow direction, *cf.* Fig. 7) it is necessary to introduce a slip tensor as argued by Bazant & Vinogradova.<sup>47</sup> Equation (5) can be interpreted as an asymptotic approximation to treat configurations for which either the continuum equations break down, or the surface geometry presents a microstructure.

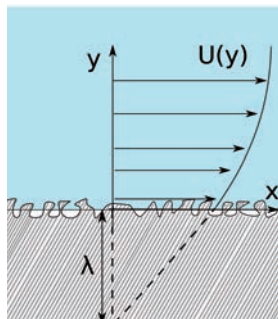


Fig. 9 – Schematic of the Navier slip length. The choice of where to position the x-axis is arbitrary and the slip length depends on it; a common choice is to put the  $y = 0$  reference axis just on top of the most protruding roughness element(s).



Situations where the slip length does not vanish include the flow of an advancing free surface, such as that developing when a drop of liquid flows down an incline under gravity, or the motion in micro- and nano-fluidic devices. In the first instance it has been shown<sup>48</sup> that a contact line singularity develops, with stresses and viscous dissipation in the fluid wedge bordered by the solid and the liquid-gas interface growing without bound under the usual no-slip condition. Remedies within the continuum model include (i) the use of a thin precursor film upstream of the advancing front, or (ii) the use of a slip boundary condition in the proximity of the triple point. In the case of micro- or nano-fluidic apparatuses, provided the Knudsen number exceeds a value around 0.1, slip has been shown to be important,<sup>49</sup> at least for solid surfaces which are not atomically smooth.

The widespread use of miniaturized devices for a variety of medical and engineering applications renders the employment of SH materials of interest, with slip lengths used to enhance flow rates for a given pressure gradient (or conversely, reduce the pressure drop necessary to pump a given flow). A simple example can illustrate this effect: let us consider a micro-channel bounded by two infinite parallel plates distant  $2H$ , the lower one of which (at  $y = -H$ ) can support slip. A fluid of dynamic viscosity  $\mu$  ( $\mu = \rho\nu$ , with  $\rho$  the fluid density and  $\nu$  its kinematic viscosity) can flow in the channel under the action of a pressure gradient  $-\frac{dp}{dx}$ ; then, the bulk speed within the channel increases with the slip length  $\lambda$  as

$$\bar{U} = \frac{2H^2}{3\mu} \left( -\frac{dp}{dx} \right) \frac{H + 2\lambda}{2H + \lambda}. \quad (6)$$

When expressed in terms of the mean velocity for the no-slip case,  $\bar{U}_{\lambda=0}$ , it is

$$\bar{U} = \bar{U}_{\lambda=0} \frac{2(H + 2\lambda)}{2H + \lambda},$$

which shows that, if  $\lambda$  is rendered equal to, for example, the half-channel thickness  $H$ , the volumetric flow rate through the channel is twice that of the no-slip case. The slip velocity at the SH wall is:

$$U(y = -H) = \bar{U} \frac{3\lambda}{H + 2\lambda};$$



this is also a growing function of  $\lambda$  and attains the value  $\bar{U}$  when  $\lambda = H$ . This simple example shows the interest of finding means to increase  $\lambda$  through the interplay of wettability and surface roughness.

### 2.1 The effective surface slip length

Effective slip boundary conditions have been proposed for a few periodic microstructures, under the hypothesis that the fakir state is maintained with planar, no-shear liquid-gas interfaces. Thus, alternating no-slip and no-shear boundary conditions are enforced on planes above which the liquid satisfies the creeping flow equations.

Different planar lattices have been studied: Philip<sup>50</sup> has studied the case of periodic ridges both aligned and perpendicular to the mean stream. The effective (*i.e.* valid in an averaged sense) slip length in the second case is half that of the first, for the same values of  $w$  and  $b$  (*cf.* Fig. 3 for notations). Ng & Wang<sup>51</sup> have evaluated  $\lambda$  for both square arrays of posts, emerging from the substrate, and holes, carved in the substrate. Davis and Lauga<sup>52,53</sup> have studied circular posts in both square and rectangular arrays, as well as a grid-like structure. The slip length  $\lambda$ , normalized by the lattice periodicity  $b$ , is given as function of  $\phi_s$ , the solid area fraction of the surface, in both Tab. 1 and in Fig. 10 for some representative cases. The validity of the results reported in Tab. 1 is typically limited to values of  $\phi_s$  up to 0.25.

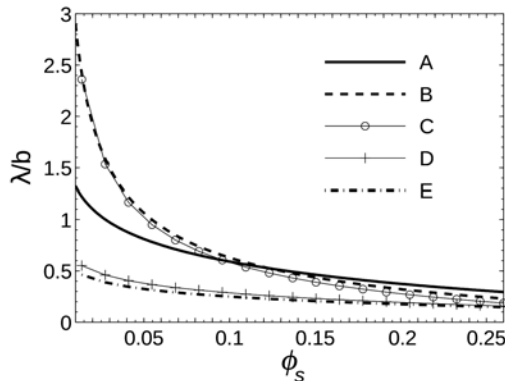
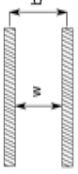

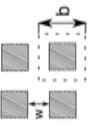

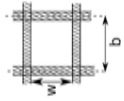


Fig. 10 – Dimensionless effective slip length as a function of the solid area fraction for a few regular SH lattices (identified by the letters **A** through **E** in Tab. 1).

Tab. 1 – Normalized effective slip lengths (column to the right) for a few rough-surface patterns in the fakin state. The no-slip region is shown with hatched lines, while the shear-free region is white.

<p>A. Ridges aligned with the flow (Philip<sup>50</sup>)</p>		$\phi_s = 1 - \frac{w}{b}$	$\frac{\lambda}{b} = \frac{1}{\pi} \ln \left\{ \sec \left[ \frac{\pi}{2} (1 - \phi_s) \right] \right\}$
<p>B. Circular posts in a square lattice (Davis &amp; Lauga<sup>53</sup>)</p>		$\phi_s = \frac{\pi}{4} \left( 1 - \frac{w}{b} \right)^2$	$\frac{\lambda}{b} = 0.332 \phi_s^{-1/2} - 0.421$
<p>C. Square posts in a square lattice (Ng &amp; Wang<sup>51</sup>)</p>		$\phi_s = \left( 1 - \frac{w}{b} \right)^2$	$\frac{\lambda}{b} = 0.33 \phi_s^{-1/2} - 0.461$
<p>D. Circular cavities in a square lattice (Ng &amp; Wang<sup>51</sup>)</p>		$\phi_s = 1 - \frac{\pi}{4} \left( \frac{w}{b} \right)^2$	$\frac{\lambda}{b} = -0.134 \ln \phi_s - 0.023$
<p>E. Grid-like pattern (Davis &amp; Lauga<sup>52</sup>)</p>		$\phi_s = 1 - \left( \frac{w}{b} \right)^2$	$\frac{\lambda}{b} = -0.107 \ln \phi_s + 0.003$

It is consistently found that slip increases with the reduction in solid area fraction and that  $\lambda$  is of order b. Square and circular posts yield the largest slip for  $\phi_s < 0.1$ , whereas ridges aligned along the stream provide the best result for larger values of the solid area fraction. A grid-like structure (*i.e.* square cavities carved in the substrate) yields the lowest values of  $\lambda$ , probably coupled to a good capacity of trapping and maintaining air bubbles within.

After the wetting transition, the boundary conditions at a wall with regularly patterned roughness can be expressed via two coefficients, a *protrusion* coefficient accounting for the effect of the aspect ratio of the individual roughness element, and a *proximity* coefficient which considers the mutual interference of multiple wall perturbations placed in a periodic array.<sup>54</sup> The coefficients proposed by Luchini<sup>54</sup> can be used to assess the reduction in slip lengths for the Wenzel state as compared to the Cassie-Baxter state, for selected surface topographies.

### 3. TRANSITION AND TURBULENCE WITH SLIP CONDITIONS

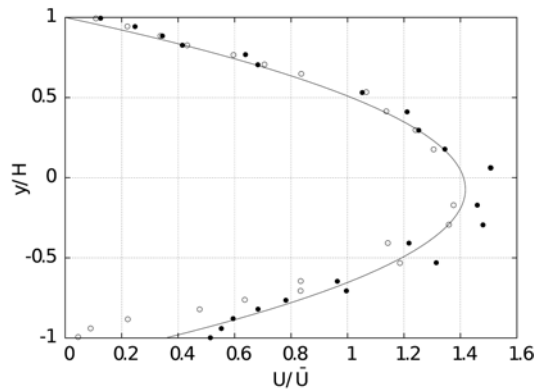
Transition and turbulence are open issues even for simple, no-slip, plane shear flows, such as the Couette or Poiseuille cases, despite the advances made in the last twenty years with direct numerical simulations, with advanced experimental techniques, and with the new understanding provided by the effect of nonnormality on the initial growth of disturbance waves. Some reliable experimental and numerical results have appeared very recently for the case of SH surfaces.

#### 3.1 Some linear stability results

Let us take as a reference the case studied via microparticle image velocimetry ( $\mu$ -PIV) by Ou, Perot & Rothstein<sup>55</sup> and Ou & Rothstein,<sup>56</sup> and focus on the linear stability of the flow in the micro-channel bounded by two walls at  $\pm H$ , the lower one of which can support slip. The streamwise velocity distribution in the channel is

$$\frac{U(y)}{\bar{U}} = \frac{3(2H + 3\lambda) - 2\lambda\frac{y}{H} - (2H + \lambda)\left(\frac{y}{H}\right)^2}{H + 2\lambda}, \quad (7)$$

with the velocity scale  $\bar{U}$  given in equation (6). This velocity distribution is displayed in *Fig. 11* together with the experimental values by Ou & Rothstein;<sup>56</sup> their data have been digitized from *Fig. 10* of their article, without the error bars on the dimensionless velocity (the largest value of which is equal to 0.3, close to the channel axis). Another case studied experimentally by Ou, Perot & Rothstein<sup>55</sup> considers longitudinal ridges in a channel of thickness  $2H = 127 \mu\text{m}$ , with width  $w$  of the ridges equal to either 20, 40 or  $80 \mu\text{m}$  and spanwise periodicity  $b$  equal to 40, 60 or  $100 \mu\text{m}$ . According to the theory by Philip,<sup>50</sup> the slip lengths in these three cases should be  $\lambda = 4.4, 13.2$  and  $37.4 \mu\text{m}$ , in reasonably good agreement to the values found indirectly by Ou and colleagues through pressure drop experiments, which are, respectively, 6, 12 and  $24 \mu\text{m}$ . Discrepancies can partly be ascribed to the deflection of the air-water interface in the experiments.



*Fig. 11* – Velocity distribution in a microchannel with a lower slip wall. The microchannel of the experiments by Ou & Rothstein<sup>56</sup> has a thickness  $2H = 85 \mu\text{m}$ ; the lower wall has microridges aligned along the flow direction, with  $w = 30 \mu\text{m}$  and  $b = 60 \mu\text{m}$  (cf. Tab. 1 for definitions). The two sets of experimental values correspond to  $\mu$ -PIV measurements taken above the center of the ridge (o) and above the center of the air-water interface (●). The continuous line through the experimental data points is given by equation (7) with  $\lambda = 6.6 \mu\text{m}$  as predicted by Philip.<sup>50</sup>

Conventional linear stability analysis can be easily carried out by assuming two-dimensional infinitesimal disturbances in the form of normal modes, *i.e.*

$$\tilde{f}(t, x, y) = f(y) \exp(\sigma t + i\alpha x);$$

with  $\tilde{f}$  the generic disturbance,  $\alpha$  the (real) streamwise wavenumber and  $\sigma$  the (complex) growth rate. It is easy to recover the Orr-Sommerfeld equation for the vertical disturbance velocity  $v$ , together with four boundary conditions:

$$v = v' = 0 \text{ at } y = H,$$

$$v = v' - \lambda v'' = 0 \text{ at } y = -H,$$

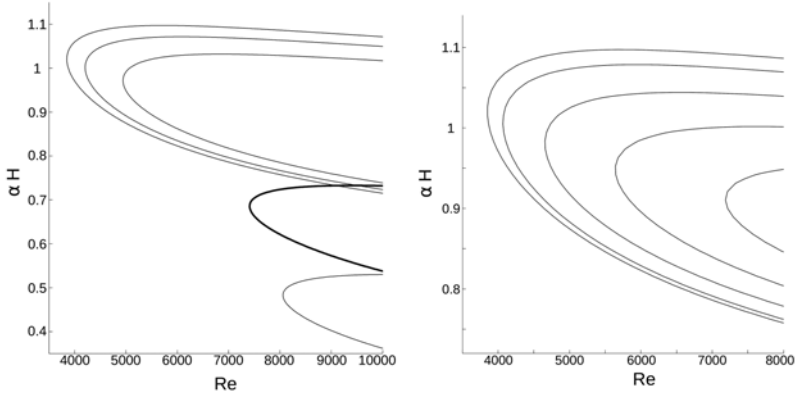
with primes used to denote derivation with respect to the independent variable  $y$ . The slip conditions above are adequate as long as  $2\pi/\alpha$  is much larger than the characteristic dimension  $b$  of the SH micro-texture. In the boundary conditions there is a single slip length  $\lambda$  since disturbances are taken in the form of waves travelling only along  $x$ ; in the case of oblique waves, a second, and possibly different, slip length would have been necessary to express the  $z$ -component of the disturbance velocity at the reference surface. Neutral stability curves for varying  $\lambda/H$ 's are plotted in *Fig. 12* (including also the case of two slip walls, right frame of the figure), highlighting the stabilizing effect of SH surfaces.

For the case studied by Ou & Rothstein<sup>56</sup> ( $\lambda/H = 0.1553$ ) the onset of two-dimensional Tollmien-Schlichting waves is postponed from  $Re = 3848$  to  $7409$  ( $Re$  is defined by  $\bar{U}H/\nu$ ), with the characteristic wavelength of the modal disturbance increasing rapidly past  $\lambda$  around  $0.07 H$ , a sign of the modified interplay between mean flow and disturbance field around the critical layer. By way of example, when  $\lambda/H = 0.07$  the critical Reynolds number and wavenumber are, respectively,  $Re_c = 9617$  and  $\alpha_c = 0.80/H$ ; in this case the phase velocity is  $0.326$  times the mean velocity  $\bar{U}$ , and the critical layer is placed  $0.056 H$  away from the SH wall (and over twice this length on the side of the no-slip wall).

If both channel walls are rendered SH the onset of Tollmien-Schlichting waves is considerably postponed, as exemplified by *Fig. 12* (right frame), in agreement with results by Min & Kim<sup>57</sup> and Lauga & Cossu.<sup>58</sup>

Beyond indicating the enhanced delay of the Tollmien-Schlichting transition for the case of a channel with *two* SH walls, the results demonstrate that a significant effect can be expected only in microdevices. The largest possible slip length ever reported<sup>16</sup> is close to  $400 \mu m$ , obtained by carefully nanostructuring the sidewalls of flow-aligned

ridges with pitch  $b$  equal to  $450 \mu m$  and solid area fraction  $\phi_s = 2\%$ , coherent with the results in *Fig. 10*. Taking this as the upper limit case, and considering, for example, a channel with two SH walls distant  $2H = 16 cm$ , it is  $\lambda/H = 0.005$ ; this corresponds to the second curve from the left in *Fig. 12* (right frame), too close to the curve of the no-slip case for stabilization to be of any practical relevance.



*Fig. 12* – Neutral stability curves for the flow in a micro-channel with one (left frame) or both (right frame) slip walls; the unstable region for each value of  $\lambda$  is contained within the area embraced by each curve. In the left frame the values of  $\lambda/H$  are, from top to bottom, 0, 0.01, 0.02, 0.1553 and 0.3; for the conditions of the experiments by *Ou & Rothstein*<sup>56</sup> the neutral curve is drawn with a thick line. For the results on the right frame, the base flow is given by  $U(y) = 1.5 \bar{U} [1 + 2\lambda/H - y^2/H^2] / (1 + 3\lambda/H)$ , and the slip boundary conditions for the vertical disturbance velocity component are  $[v' \pm \lambda w']_{\pm H} = 0$ . From left to right:  $\lambda/H = 0, 0.005, 0.01, 0.015, 0.02$ .

A few open issues remain relative to the role of non-modal, transiently growing disturbances on the threshold for turbulent transition, particularly when nonlinear effects are accounted for. Preliminary results, both in the linear and nonlinear regimes, have been reported by *Min & Kim*.<sup>57</sup> In the linear case, the presence of a SH surface has insignificant consequences as long as  $\lambda$  is much smaller than  $H$  (*cf.* also *Lauga & Cossu*<sup>58</sup>). On the other hand, even a small streamwise slip has a remarkable effect on transition delay when the disturbance amplitude is sufficiently large, whereas spanwise slip appears to trigger early transition. Preliminary experimental results on transition delay for the turbulent boundary layer developing over a SH plate have been reported recently by *Lyu et al.*<sup>59</sup> More work is however necessary to elucidate the

mechanisms of transition in the nonlinear regime, for isotropic and anisotropic surface patterns.

### 3.2 Turbulence

The literature reports some very recent, promising results, both experimental and numerical, for the effect of superhydrophobicity on drag reduction.

For the case of a channel flow with microridges aligned in the flow direction, Park, Park & Kim<sup>60</sup> have discovered, via direct numerical simulations, that the skin friction drag decreases significantly when the slip length is at least of the order of the viscous sub-layer thickness, *i.e.*  $\lambda^+ = \lambda u_\tau / \nu \approx 5$ ; drag is progressively reduced upon further increase of  $\lambda^+$ , until saturation at  $\lambda^+ \approx 30 - 40$ , with a significant modification of the near-wall turbulent structures. For the case of surface ridges aligned with the mean flow, and considering the laminar results in *Fig. 10* just to have an order of magnitude for  $b^+$ , it can be speculated that a drag-reducing effect might subsist even in the Wenzel state, at least in a range of speeds, simply by exploiting the *riblet effect* (*cf.* Section 1.2). Experiments of riblet-ed surfaces, coated with a sub-micrometric layer of a hydrophobic polymer, tested in a cone-and plate rheometer system have recently revealed a drag reduction in the turbulent regime of up to 20%, compared to the base, smooth-surface case.<sup>61</sup>

Microridges aligned with the main flow have also been examined experimentally by Park, Sun & Kim<sup>35</sup> in a turbulent boundary layer; they carefully monitored the state of the gas within the ridges and studied cases with different solid area fraction. Their set up considers a side-by-side configuration of smooth and superhydrophobic sample surfaces (of dimensions  $20 \text{ mm} \times 10 \text{ mm}$ ) flush-mounted on the upper wall of a water-tunnel test section, and the (surface integrated) shear stress is assessed by suspending the two samples with an identical set of flexure beam springs and measuring the differential displacement. For  $\phi_s = 0.05$  a drag reduction equal to 75% is obtained at  $Re_\tau \approx 250$  (based on boundary layer thickness and friction velocity).

As expected, the drag-reducing effect is enhanced by increasing the periodicity  $b$  of the microridges, and is mitigated by raising  $\phi_s$ 's.

Park, Sun & Kim<sup>35</sup> have been unable to evaluate the slip length, because of spatial resolutions problems with the laser Doppler velocimetry (LDV) system employed. Such a value is available with  $\mu$ -



PIV, which allows a spatial resolution of the order of  $1\ \mu\text{m}$ ,<sup>62</sup> and possibly with digital holographic microscopy.<sup>63</sup>

Moving to a less academic configuration, Dong *et al.*<sup>64</sup> have recently reported 40% drag reduction for the case of a macroscopic model ship tested in a 6 m-long water tunnel, both with and without a micro- and nano-patterned SH coating. The result is very encouraging, since the drag in this case includes a sizeable part of wave drag, unaffected by the coating. However, the tests' duration is of only a few seconds and no mention is made of the longevity of the gas layer. This is, in fact, the main limiting factor for practical applications. The pressure difference between the liquid and gas phases holds primary responsibility for the collapse of the Cassie-Baxter state; the wetting transition is also favoured by the flow of gas across neighboring micro-channels (when interconnected), and by the solubility of the trapped gas in the surrounding liquid. Active or passive means to supply gas to an already wetted rough surface might be envisioned, and dewetting has shown to be possible, provided the wall microstructures satisfy certain geometrical constraints.<sup>65</sup> Partial recovery can be achieved by entraining outside air, as shown by Lee & Kim,<sup>66</sup> but this works only for small, above-ambient, water pressures. Another promising approach, which remains effective under large liquid pressures, consists in placing electrodes on the substrate of the SH surface, and using electrolysis to replenish the lost gas.<sup>65,66</sup>

#### 4. BIOFOULING

All naval vessels suffer consequences from the phenomenon of biofouling, a very rapid process (*cf. Fig. 13*) which initiates with the formation of a biofilm to which larger organisms, such as barnacles, can later attach. It is known that heavy calcareous fouling can increase the required shaft power of a ship by 86% as compared to a hydraulically smooth hull at cruising speed,<sup>67</sup> so that the application of anti-fouling coatings is a necessity.

Biocides have been successfully used in the past to regulate fouling; in particular, tributyltin (TBT)-containing paint formulations, developed in the 1970s, were so effective at reducing fouling that no further paint development was considered necessary. However, the toxicity of TBT led to a worldwide ban on the use of these compounds in

2008,<sup>68</sup> which spurred research into alternative and environmentally benign biofouling solutions. Current strategies include both hydrophobic (fluoropolymers and silicone) and hydrophilic (glycine betaine and sulfobetaine) coatings; in the first instance a smooth surface is created which aims to prevent the attachment of larger microorganisms, while in the second the high hydration of the surface increases the energetic penalty of removing water for proteins and microorganisms to attach.

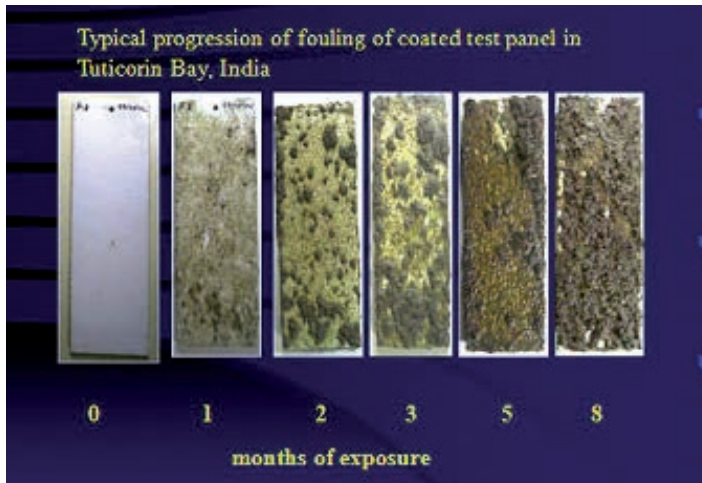


Fig. 13 – Fouling over time at a field test site in southern India.  
Image from <http://www.poseidonsciences.com/static/immersion.html>.

Very recently, the Japanese company *Nippon Paint Marine* has patented and put into commerce a painting called A-LF-Sea based on copper silyl acrylate, for antifouling, and hydrogel particles, to realise a liquid-to-liquid near-wall shear layer. The special kind of hydrogel employed is composed of a polymeric network able to absorb water from the outside, until saturation, and capable to retain it with little swelling. This latter characteristic renders it suitable for anti-fouling coatings. According to the manufacturer, by treating a flat surface with A-LF-Sea, and by exploiting the liquid-to-liquid effect, frictional drag is reduced by 15%, which would result in a reduction of approximately 10% of the total resistance of a ship. This coating has been applied to over 140 ships in the period that goes from April 2013 to April 2014, and the beneficial effects are currently being evaluated in a cooperation between *Nippon Paint Marine* and *Kobe University*.

## 5. CONCLUDING REMARKS

Much progress has been made in the understanding of superhydrophobicity since the works by Wenzel<sup>9</sup> and Cassie & Baxter,<sup>12</sup> but more is needed to be able to design and apply SH coatings to submerged objects with full confidence on both the drag-reducing effect and its durability. Producing a SH surface is relatively easy and several different approaches have been proposed in the literature; the main technological challenge is related to the longevity of the Cassie-Baxter state, when the superhydrophobic surface is subject to external pressure and shear. Until now, longevity of laboratory-developed coatings is of the order of a few days; this duration has to be extended by a factor of 100 and more, in order to render the technique of interest to the naval industry, otherwise a dewetting strategy might be indispensable. Other issues rest with the cost, ease of large-scale application, and resistance to wear. A new anti-fouling paint developed by the company Nippon Paint Marine ([http://nipponpaint-marine.com/en/products/a\\_lf\\_sea/index.html](http://nipponpaint-marine.com/en/products/a_lf_sea/index.html)) seems to meet some industrial expectations, but care is needed not to interpret marketing boasts as reliable laboratory results.

The ingredients which emerge for the design of effective coatings for real-world underwater implementation appear to be the following:

- The coating should have a (regular or irregular) fibrous polymeric structure of sub-millimetric characteristic dimensions, with embedded smaller-scale features. This could possibly be achieved by the simple mechanical abrasion of the low-surface-energy material.
- The solid area fraction of the surface  $\phi$ , should be as low as possible for large slip lengths to be attained.
- It is probably advantageous to use hydrophilic patches on top of the microroughness elements (on those parts in direct contact with the liquid) to pin and stabilize the air-water interface.
- A system of micro-barriers transverse to the main water flow should be envisioned to prevent air from escaping sideways, thus promoting the longevity of the air layer.
- The use of an active dewetting system could be considered, possibly based on electrolytically generated gas. Maintaining the gas layer is crucial also to inhibit biofouling activity and metal surface corrosion, thanks to the reduced areas of contact between the solid surface and water.
- An alternative for naval applications, when a constant speed is main-

tained over a long time, could be constituted by a *porous*, riblet-like topography (*cf.* Fig. 5, right), still with embedded smaller-scale (nano) features. This might permit to take advantage of superhydrophobicity before the wetting transition has occurred, and of the drag-reducing effect of riblets when in the Wenzel state. Moreover, active and passive gas replenishing systems, which take advantage of the porous nature of the surface, can be envisioned (a MURI - Multidisciplinary University Initiative - led by Prof. S.L. Ceccio of the University of Michigan, has been recently sponsored by the US Office of Naval Research to look - among other things - into these aspects; *cf.* <https://onrsuperhydrophobic.org/>).

The goal of the research community is to identify low cost technologies to deliver on the points above. This is an exciting task because of the tremendous benefits expected; for example, in the maritime transport sector, skin friction drag contributes to over 60% of the total drag for a cargo ship and 80% for a tanker.<sup>69</sup> Lowering drag by even a small amount would have a global impact on energy saving and greenhouse gas reduction.

#### ACKNOWLEDGEMENTS

Several colleagues have contributed through discussions and interactions to the present work, including in particular F. Barberis, C. Boragno, M. Capurro, P. Luchini, N. Mazellier, A. Mazzino, D. Natali, J. Pralits, A. Ungaro, and G. Zampogna. The support of the *Istituto Lombardo, Accademia di Scienze e Lettere* and of the *Edoardo Kramer Foundation*, through the “2013 Kramer Award”, is very gratefully acknowledged. The activity on SH coatings has started thanks to a *Fincantieri Innovation Challenge* grant, monitored by Cetena S.p.A. (with G. Caprino as program officer).

#### REFERENCES

- [1] E. Inoue. On the turbulent structure of air flow within crop canopy. *J. Meteorol. Soc. Jpn.*, 1:317-346, 1963.
- [2] J.J. Finnigan. Waving plants and turbulent eddies. *J. Fluid Mech.*, 652:1-4, 2010.
- [3] J. Oeffner and G.V. Lauder. The hydrodynamic function of shark skin and two biomimetic applications. *J. Exp. Biology*, 215:785-795, 2012.

- 
- [4] L. Wen, J.C. Weaver, and G.V. Lauder. Biomimetic shark skin: design, fabrication and hydrodynamic function. *J. Exp. Biol.*, 217:1656-1666, 2014.
- [5] The word *apparent* is used with reference to the macroscopic measure of the contact angle; such a measure would change if we progressively zoomed on the contact line down to the molecular scale.
- [6] T. Young. An essay on the cohesion of fluids. *Phil. Trans. R. Soc. Lond.*, 95:65-87, 1805.
- [7] The prefix “hydro” indicates that the liquid considered - in the original usage of the words hydrophobic and hydrophilic - was water.
- [8] F. Barberis and M. Capurro. Wetting in the nanoscale: A continuum mechanics approach. *J. Colloid Interf. Sci.*, 326:201-210, 2008.
- [9] R.N. Wenzel. Resistance of solid surfaces to wetting by water. *Industr. and Eng. Chemistry*, 28(8):988-994, 1936.
- [10] G. Wolansky and A. Marmur. Apparent contact angles on rough surfaces: the Wenzel equation revisited. *Colloids and Surfaces A*, 156:381-388, 1999.
- [11] L. Gao and T.J. McCarthy. How Wenzel and Cassie were wrong. *Langmuir*, 23:3762-3765, 2007.
- [12] A.B.D. Cassie and S. Baxter. Wettability of porous surfaces. *Trans. Faraday Soc.*, 40:546-551, 1944.
- [13] D. Quéré. Fakir droplets. *Nature Materials*, 1:14-15, 2002.
- [14] D. Quéré. Wetting and roughness. *Annu. Rev. Mater. Res.*, 38:71-99, 2008.
- [15] Y. Yu, Z.-H. Zhao, and Q.-S. Zheng. Mechanical and superhydrophobic stabilities of two-scale surfacial structure of lotus leaves. *Langmuir*, 23:8212-8216, 2007.
- [16] C. Lee and C.-J. Kim. Maximizing the giant liquid slip on superhydrophobic microstructures by nanostructuring their sidewalls. *Langmuir*, 25:12812-12818, 2009.
- [17] Y. Su, B. Ji, K. Zhang, H. Gao, Y. Huang, and K. Hwang. Nano to micro structural hierarchy is crucial for stable superhydrophobic and water-repellent surfaces. *Langmuir*, 26:4984-4989, 2010.
- [18] E. Bormashenko. Progress in understanding wetting transitions on rough surfaces. *Adv. Colloids Interf. Sci.*, in press, 2014.
- [19] E. Bormashenko, Y. Bormashenko, T. Stein, G. Whyman, and E. Bormashenko. Why do pigeon feathers repel water? Hydrophobicity of penna, Cassie-Baxter wetting hypothesis and Cassie-Wenzel capillarity-induced wetting transition. *J. Colloid Interf. Sci.*, 311:212-216, 2007.
- [20] W. Barthlott and C. Neinhuis. Purity of the sacred lotus, or escape from contamination in biological surfaces. *Planta*, 202:1-8, 1997.
- [21] N.J. Shirtcliffe, G. McHale, M.I. Newton, G. Chabrol, and C.C. Perry. Dual-scale roughness produces unusually water-repellent surfaces. *Adv. Mater.*, 16:1929-1932, 2004.
- [22] W. Barthlott, T. Schimmel, S. Wiersch, K. Koch, M. Brede, M. Barczewski, S. Walheim, A. Weis, A. Kaltenmaier, A. Leder, and H.F. Bohn. The *salvinia* paradox: Superhydrophobic surfaces with hydrophilic pins for air retention under water. *Adv. Mater.*, 22:2325-2328, 2010.

- 
- [23] D.L. Hu, B. Chan, and J.W.M. Bush. The hydrodynamics of water strider locomotion. *Nature*, 424:663-666, 2003.
- [24] X. Gao and L. Jiang. Biophysics: water-repellent legs of water striders. *Nature*, 432:36, 2004.
- [25] P. Ditsche-Kuru, E.S. Schneider, J.-E. Melskotte, M. Brede, A. Leder, and W. Barthlott. Superhydrophobic surfaces of the water bug *notonecta glauca*: a model for friction reduction and air retention. *Beilstein J. Nanotech.*, 2:137-144, 2011.
- [26] Y. Fang, G. Sun, TQ. Wang, Q. Cong, and LQ. Ren. Hydrophobicity mechanism of non-smooth pattern on surface of butterfly wing. *Chinese Sci. Bull.*, 52:711-716, 2007.
- [27] M.J. Walsch. Riblets as a viscous drag reduction technique. *AIAA J.*, 21:485-486, 1983.
- [28] P. Luchini, F. Manzo, and A. Pozzi. Resistance of a grooved surface to parallel flow and cross-flow. *J. Fluid Mech.*, 228:87-109, 1991.
- [29] D.W. Bechert, M. Bruse, W. Hage, J.G.T. Van der Hoeven, and G. Hoppe. Experiments on drag-reducing surfaces and their optimization with an adjustable geometry. *J. Fluid Mech.*, 338:59-87, 1997.
- [30] M. Ma and R.M. Hill. Superhydrophobic surfaces. *Current Opinion in Colloid and Interf. Sci.*, 11:193-202, 2006.
- [31] X. Zhang, F. Shi, J. Niu, Y. Jiang, and Z. Wang. Superhydrophobic surfaces: from structural control to functional applications. *J. Mater. Chem.*, 18:621-633, 2008.
- [32] N.J. Shirtcliffe, G. McHale, and M.I. Newton. The superhydrophobicity of polymer surfaces: recent developments. *J. Polymer Science. Part B: Polymer Physics*, 49:1203-1217, 2011.
- [33] R.J. Daniello. Drag reduction in turbulent flows over micropatterned superhydrophobic surfaces. Master's thesis, University of Massachusetts Amherst, 2009.
- [34] C. Lee and C.-J. Kim. Influence of surface hierarchy of superhydrophobic surfaces on liquid slip. *Langmuir*, 27:4243-4248, 2011.
- [35] H. Park, G. Sun, and C.-J. Kim. Superhydrophobic turbulent drag reduction as a function of surface grating parameters. *J. Fluid Mech.*, 747:722-734, 2014.
- [36] F.O. Ochanda, M.A. Samaha, H.V. Tafreshi, G.C. Tepper, and M. Gad el Hak. Fabrication of superhydrophobic fiber coatings by dc-biased ac-electrospinning. *J. Appl. Polymer Sci.*, 123:1112-1119, 2012.
- [37] R. Asmatalu, M. Ceylan, and N. Nuraje. Study of superhydrophobic electrospun nanocomposite fibers for energy systems. *Langmuir*, 27:504-507, 2011.
- [38] F. Buatier de Mongeot, D. Chiappe, F. Gagliardi, A. Toma, R. Felici, A. Garibbo, and C. Boragno. Wetting process in superhydrophobic disordered surfaces. *Soft Matter*, 6:1409-1412, 2010.
- [39] S.-H. Hsu and W.M. Sigmund. Artificial hairy surfaces with a nearly perfect hydrophobic response. *Langmuir Letter*, 26:1504-1506, 2010.
- [40] S. Srinivasan, S.S. Chhatre, J.M. Mabry, R.E. Cohen, and G.H. McKinley. Solution spraying of poly(methyl methacrylate) blends to fabricate microtextured, superoleophobic surfaces. *Polymer*, 52:3209-3218, 2011.
- [41] S. Srinivasan, W. Choi, K.C. Park, S.S. Chhatre, R.E. Cohen, and G.H.

- McKinley. Drag reduction for viscous laminar flow on spray-coated non-wetting surfaces. *Soft Matter*, 9:5691-5702, 2013.
- [42] J.E. Rodriguez, A.M. Anderson, and M.K. Carroll. Hydrophobicity and drag reduction properties of surfaces coated with silica aerogels and xerogels. *J. Sol-Gel Sci. Technol.*, 71:490-500, 2014.
- [43] M.A. Nilsson, R.J. Daniello, and J.P. Rothstein. A novel and inexpensive technique for creating superhydrophobic surfaces using Teflon and sandpaper. *J. Phys. D: Appl. Phys.*, 43:045301, 2010.
- [44] D. Song, R.J. Daniello, and J.P. Rothstein. Drag reduction using superhydrophobic sanded Teflon surfaces. *Exp. Fluids*, 55:1783, 2014.
- [45] G.I. Taylor. Stability of a viscous liquid contained between two rotating cylinders. *Phil. Trans. Royal Soc. London, Ser. A*, 223:289-343, 1923.
- [46] C.L.M.H. Navier. Mémoire sur les lois du mouvement des fluides. *Mem. Acad. R. Sci. Inst. France*, 6:389-440, 1823.
- [47] M.Z. Bazant and O.I. Vinogradova. Tensorial hydrodynamic slip. *J. Fluid Mech.*, 613:125-134, 2008.
- [48] C. Huh and L.E. Scriven. Hydrodynamic model of steady movement of a solid/liquid/fluid contact line. *J. Colloid Interf. Sci.*, 35:85-101, 1971.
- [49] G. Karniadakis, A. Beskok, and N. Aluru. *Microflows and Nanoflows: Fundamentals and Simulation*. Springer, 2006.
- [50] J.R. Philip. Flows satisfying mixed no-slip and no-shear conditions. *J. Applied Math. Phys. (ZAMP)*, 23:353-372, 1972.
- [51] C.-O. Ng and C.Y. Wang. Apparent slip arising from Stokes shear flow over a bidimensional patterned surface. *Microfluid. Nanofluid.*, 8:361-371, 2010.
- [52] A.M.J. Davis and E. Lauga. The friction of a mesh-like super-hydrophobic surface. *Phys. Fluids*, 21:113101, 2009.
- [53] A.M.J. Davis and E. Lauga. Hydrodynamic friction of fakir-like superhydrophobic surfaces. *J. Fluid Mech.*, 661:402-411, 2010.
- [54] P. Luchini. Linearized no-slip boundary conditions at a rough surface. *J. Fluid Mech.*, 737:349-367, 2013.
- [55] J. Ou, B. Perot, and J.P. Rothstein. Laminar drag reduction in microchannels using ultrahydrophobic surfaces. *Phys. Fluids*, 16:4635-4643, 2004.
- [56] J. Ou and J.P. Rothstein. Direct velocity measurements of the flow past drag-reducing ultrahydrophobic surfaces. *Phys. Fluids*, 17:103606, 2005.
- [57] T. Min and J. Kim. Effects of hydrophobic surface on stability and transition. *Phys. Fluids*, 17:108106, 2005.
- [58] E. Lauga and C. Cossu. A note on the stability of slip channel flows. *Phys. Fluids*, 17:088106, 2005.
- [59] S. Lyu, D.C. Nguyen, D. Kim, W. Hwang, and B. Yoon. Experimental drag reduction study of super-hydrophobic surface with dual-scale structures. *Applied Surface Science*, 286:206-211, 2013.
- [60] H. Park, H. Park, and J. Kim. A numerical study of the effects of superhydrophobic surface on skin-friction drag in turbulent channel flow. *Phys. Fluids*, 25:110815, 2013.



- [61] C. Barbier, E. Jenner, and B. D'Urso. Large drag reduction over superhydrophobic riblets. *arXiv:1406.0787v1*, 2014.
- [62] R.J. Daniello, N.E. Waterhouse, and J.P. Rothstein. Drag reduction in turbulent flows over superhydrophobic surfaces. *Phys. Fluids*, 21:085103, 2009.
- [63] J. Katz and J. Sheng. Applications of holography in fluid mechanics and particle dynamics. *Annu. Rev. Fluid Mech.*, 42:531-555, 2010.
- [64] H. Dong, M. Cheng, Y. Zhang, H. Wei, and F. Shi. Extraordinary drag-reducing effect of a superhydrophobic coating on a macroscopic model ship at high speed. *J. Mater. Chem. A*, 1:5886-5891, 2013.
- [65] C. Lee and C.-J. Kim. Underwater restoration and retention of gases on superhydrophobic surfaces for drag reduction. *Phys. Rev. Lett.*, 106:014502, 2011.
- [66] C. Lee and C.-J. Kim. Wetting and active dewetting processes of hierarchically constructed superhydrophobic surfaces fully immersed in water. *J. Microelectromech. Systems*, 21:712-720, 2012.
- [67] M.P. Schultz. Effects of coating roughness and biofouling on ship resistance and powering. *Biofouling*, 23:331-341, 2007.
- [68] S. Sonak. Implications of organotin in the marine environment and their prohibition. *J. Environ. Manage.*, 90:S1-S3, 2009.
- [69] K. Fukuda, J. Tokunaga, T. Nobunaga, T. Nakatani, T. Iwasaki, and Y. Kunitake. Frictional drag reduction with air lubricant over a super-water-repellent surface. *J. Mar. Sci. Technol.*, 5:123-130, 2000.